Res Chem Intermed (2018) 44:721–738
https://doi.org/10.1007/s11164-017-3130-1

Synthesis, structural characterization, and Hirshfeld surface analysis of three cocrystals based on flexible bis(benzimidazole) derivatives with aromatic carboxylic acids

Jing-Wang Cui[1] · Yan-Qin Zhao[1] · Zeng-Chuan Hao[1] · Guang-Hua Cui[1]

Received: 22 March 2017 / Accepted: 22 August 2017 / Published online: 31 August 2017

Abstract Based on 1,3-bis(2-methylbenzimidazole)propane (L1), 1,4-bis(2-methylbenzimidazole)butane (L2) and 1,4-bis(2-methylbenzimidazol-1-ylmethyl) benzene (L3) with aromatic carboxylic acids, three cocrystals, $[(H_2L1)^{2+}\cdot 2(H_2btrc)^{1-}]$ (**1**), $[(H_2L2)^{2+}\cdot(H_2btec)^{2-}\cdot 2H_2O]$ (**2**) and $[(H_2L3)^{2+}\cdot(H_2btec)^{2-}]$ (**3**) (H_3btrc = 1,2,4-benzenetricarboxylic acid, H_4btec = 1,2,4,5-benzenetetracarboxylic acid) were synthesized in solution and obtained by slow evaporation. All solid products were characterized by elemental analyses, IR spectra, and single-crystal X-ray diffraction. Components of the crystalline phase have also been investigated in terms of Hirshfeld surfaces. The bis(benzimidazole) derivatives interlinked with aromatic carboxylates through intermolecular H-bonding and π–π interactions generate diverse 3D supramolecular networks for **1**, **2**, and **3**. The Hirshfeld surfaces and 2D fingerprint plots of three cocrystals show that **1**–**3** are stabilized by N–H···O, O–H···O, and π–π intermolecular interactions. The thermal stabilities and photoluminescence properties for cocrystals **1**–**3** were presented in the solid state.

Keywords Cocrystals · Crystal structure · Fluorescence property · Hirshfeld surface · Intermolecular interaction · Thermal stability

Electronic supplementary material The online version of this article (doi:10.1007/s11164-017-3130-1) contains supplementary material, which is available to authorized users.

✉ Guang-Hua Cui
tscghua@126.com

[1] College of Chemical Engineering, Hebei Key Laboratory for Environment Photocatalytic and Electrocatalytic Materials, North China University of Science and Technology, Tangshan 063009, Hebei, People's Republic of China

Introduction

In the fields of supramolecular chemistry and crystal engineering, the design and synthesis of supramolecular compounds are of current interest due to their encouraging potential for pharmaceutical application, electrical conductivity, solid-state organic synthesis, luminescence materials, and molecular electronics [1–4]. Against this background during the past few decades, some supramolecular compounds have been successfully constructed through self-assembly adopting non-covalent intermolecular interactions [5–7]. In these non-covalent interactions, hydrogen bonds are the most powerful force for generating the supermolecule networks [8–10]. Owing to different hydrogen bonding capability, the incorporation of diverse organic building blocks with various functional groups and orientations may strongly influence the structures and properties of supramolecular compounds [11–13]. However, only limited works of the hydrogen bonding driven supramolecular architectures based on bis(benzimidazole) were reported [14–18]. In bis(2-methylbenzimidazole) derivatives, the substituent methyl of the benzimidazole ring can greatly enhance the ability of donated electrons, in both the imidazole ring and a larger conjugated π-system, that are capable of participating in hydrogen bonding and π–π stacking interactions [22, 23], which influences the resulting supramolecular architecture [19–21]. In addition, because of the ability to form strong and directional hydrogen bonds via the COOH groups, aromatic carboxylic acids, such as 1,2,4-benzenetricarboxylic acid (H_3btrc) and 1,2,4,5-benzenetetracarboxylic acid (H_4btec) (Scheme 1), are frequently used as building blocks in organic crystal engineering [1, 18, 24]. With this understanding, we choose flexible bis(benzimidazole) derivatives and aromatic carboxylic acids to generate three new cocrystals. In February 2–4, 2012, the Indo–U.S. Bilateral Meeting sponsored by the Indo–U.S. Science and Technology Forum titled *The Evolving Role of Solid State Chemistry in Pharmaceutical Science* was held in Manesar near Delhi, India. In the meeting, a more restrictive definition of cocrystal that is broader than that proposed by the

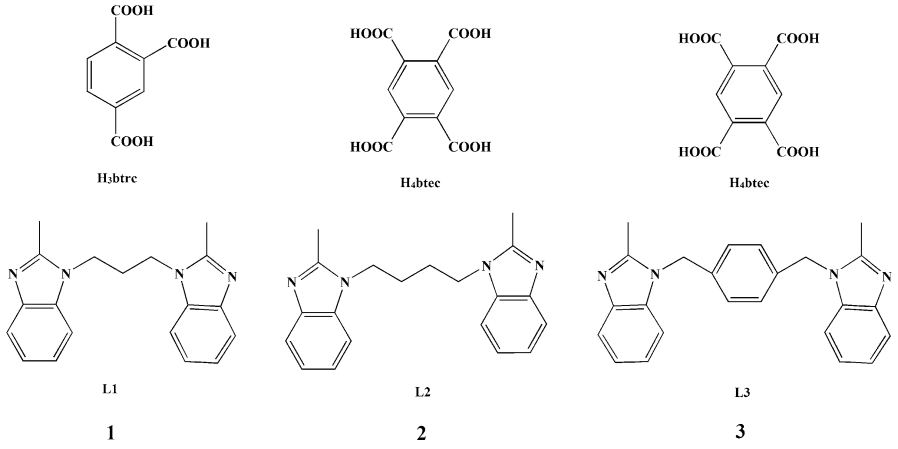

Scheme 1 The structures of the molecular components in cocrystals **1–3**

United States Food and Drug Administration (FDA) was proposed: cocrystals are solids that are crystalline single-phase materials composed of two or more different molecular and/or ionic compounds generally in a stoichiometric ratio [25].

Hirshfeld surface analysis [26, 27] represents a useful method to explore intermolecular interactions in supramolecular compounds. The surfaces encode information about all intermolecular interactions and offer a simple way to obtain information on crystal packing [28]. The breakdown of 2D fingerprint plots [29] explores the types of intermolecular contacts in supramolecular systems quantitatively and presents this information in a convenient color plot.

In order to investigate further the variations of intermolecular interactions, structures, and properties of supramolecular compounds, three new cocrystals have been successfully synthesized and characterized, namely $[(H_2L1)^{2+}\cdot 2(H_2btrc)^{1-}]$ (**1**), $[(H_2L2)^{2+}\cdot(H_2btec)^{2-}\cdot 2H_2O]$ (**2**), and $[(H_2L3)^{2+}\cdot(H_2btec)^{2-}]$ (**3**) (L1 = 1,3-bis(2-methylbenzimidazole)propane, L2 = 1,4-bis(2-methylbenzimidazole)butane, L3 = 1,4-bis(2-methylbenzimidazol-1-ylmethyl)benzene) (Scheme 1). The Hirshfeld surface-based tools are used to analyze the noncovalent forces such as hydrogen bonding and π–π interactions. Moreover, the thermal stabilities and photoluminescence properties of **1**–**3** are presented.

Experimental

Materials and measurements

All the reagents and starting materials were obtained from commercial sources and used without further purification. Melting points were obtained on a ×4 microscopic melting point apparatus made by Beijing Taike Instrument Co. and are uncorrected. C, H, and N elemental analyses were performed on a Perkin-Elmer 240C analyzer. FT-IR spectra were recorded on KBr discs using an Avatar 360 (Nicolet) spectrophotometer in the range of 4000–400 cm^{-1}. The fluorescence spectra were collected with a Hitachi F-7000 spectrophotometer at room temperature.

Preparation of the cocrystals

*$[(H_2L1)^{2+}\cdot 2(H_2btrc)^{1-}]$ (**1**)*

A mixture of L1 (30.4 mg, 0.1 mmol) and H_3btrc (42.0 mg, 0.2 mmol) was dissolved in a beaker with 15 mL methanol and 2 mL distilled water mixed solvent, and the colorless block crystals of **1** (49.5 mg) were obtained in 68.3% yield (based on 0.1 mmol L1) at ambient conditions via the slow evaporation technique. Melting point = 175–176 °C. Anal. Calcd. for $C_{37}H_{32}N_4O_{12}$ (Mr = 724.67): C 61.32, H 4.45, N 7.73%. Found: C 61.47, H 4.55, N 7.85%. IR (KBr, cm^{-1}): 3100(m), 1930(w), 1700(s), 1580(s), 1470(s), 1370(s), 1270(s), 1170(s), 1010(s), 856(m), 744(s), 633(m).

*$[(H_2L2)^{2+}\cdot(H_2btec)^{2-}\cdot 2H_2O]$ (**2**)*

The synthetic procedure of **2** was similar to **1**, except that L1 and H_3btrc were replaced by L2 (31.8 mg, 0.1 mmol) and H_4btec (25.4 mg, 0.1 mmol), respectively. Colorless block crystals of **2** (49.2 mg) were collected in 81.1% yield (based on 0.1 mmol L2). Melting point = 158–159 °C. Anal. Calcd. for $C_{30}H_{32}N_4O_{10}$ (Mr = 608.60): C 59.21, H 5.30, N 9.21%. Found: C 59.35, H 5.39, N 9.41%. IR (KBr, cm^{-1}): 3430(m), 3111(w), 1700(m), 1470(s), 1350(s), 1140(m), 1060(m), 849(m), 756(s), 650(m), 586(m), 471(w).

*$[(H_2L3)^{2+}\cdot(H_2btec)^{2-}]$ (**3**)*

The synthesis procedure of **3** was similar to **1**, except that L3 (36.6 mg, 0.1 mmol) and H_4btec (25.4 mg, 0.1 mmol) were used instead of L1 and H_3btrc, respectively. Colorless block crystals of **3** (36.8 mg) were collected in 59.3% yield (based on 0.1 mmol L3). Melting point = 146–148 °C. Anal. Calcd. for $C_{34}H_{28}N_4O_8$ (Mr = 620.60): C 65.80, H 4.55, N 9.03%. Found: C 65.97, H 4.68, N 9.11%. IR (KBr, cm^{-1}): 3095(m), 1660(s), 1550(s), 1460(w), 1400(s), 1150(m), 849(w), 746(m), 553(w).

X-ray crystallographic study

Single crystal X-ray diffraction data for cocrystals **1**–**3** were collected on a Bruker Smart 1000 CCD area-detector using graphite monochromated Mo–$K\alpha$ radiation (λ = 0.71073 Å) at 293 K with ω-scan mode. The structures were solved by direct methods, and the non-hydrogen atoms were subjected to anisotropic refinement by full-matrix least-squares on F^2 using SHELXTL package [30]. The hydrogen atoms of all water molecules were located from difference Fourier maps. The other hydrogen atoms were included in calculated position and refined with isotropic thermal parameters riding on the parent atoms. Further details of the structural analysis are summarized in Table 1. Selected bond lengths and angles for **1**–**3** are listed in Table S1. Geometrical parameters for hydrogen bonds and π–π interactions are all summarized in Table 2.

Hirshfeld surface calculations

Calculations of molecular Hirshfeld surfaces were performed by using the *CrystalExplorer* program [31, 32]. When the CIF files of cocrystals **1**–**3** were imported into the *CrystalExplorer* program, all bond lengths to hydrogen were automatically modified to typical standard neutron values (C–H = 1.083 Å, N–H = 1.009 Å, and O–H = 0.983 Å). All Hirshfeld surfaces were generated in a standard (high) surface resolution. The 3D d_{norm} surfaces are displayed using a red–white–blue colour scale, where red regions highlight shorter contacts than van der Waals (vdW) separations and a negative d_{norm} value, white regions represent the distance of contacts exactly corresponding to the vdW separations with a d_{norm} value of zero, and blue regions are for longer contacts than van der Waals (vdW)

Table 1 Crystal and refinement data for cocrystals **1–3**

	1	**2**	**3**
Empirical formula	$C_{37}H_{32}N_4O_{12}$	$C_{30}H_{32}N_4O_{10}$	$C_{34}H_{28}N_4O_8$
Formula weight	724.67	608.60	620.60
Crystal system	Triclinic	Monoclinic	Triclinic
Space group	$P\bar{1}$	$P2_1/c$	$P\bar{1}$
a (Å)	9.7105 (6)	8.8221 (3)	6.9857 (5)
b (Å)	11.3812 (9)	9.7048 (3)	9.4468 (6)
c (Å)	16.4876 (13)	16.4991 (5)	10.8032 (7)
α (deg)	77.818 (7)	90	97.504 (5)
β (deg)	85.186 (6)	99.964 (3)	91.771 (5)
γ (deg)	66.485 (7)	90	91.271 (5)
V (Å^3)	1633.2 (2)	1391.29 (8)	706.24 (8)
Z	2	2	1
D_{calc} (g/m^3)	1.474	1.453	1.459
μ (mm^{-1})	0.112	0.110	0.106
$F(000)$	756	640	324
Crystal size (mm)	0.22 × 0.19 × 0.19	0.18 × 0.17 × 0.15	0.17 × 0.16 × 0.15
Total reflections	34,196	13,599	10,923
Unique reflections	7165	2460	2886
R_{int}	0.0547	0.0377	0.0469
GOF	1.020	1.186	1.190
R_1 ($I > 2\sigma(I)$)	0.0516	0.0376	0.0473
wR_2 ($I > 2\sigma(I)$)	0.1251	0.1143	0.1420
$\Delta\rho$max (eÅ^{-3})	0.342	0.499	0.496
$\Delta\rho$min (eÅ^{-3})	−0.289	−0.655	−0.606

separations with a positive d_{norm} value. The 2D fingerprint plots are derived from the Hirshfeld surfaces by plotting the fraction of points on the surface as a function of the pair (d_i, d_e).

Results and discussion

Single crystal X-ray diffraction studies

Crystal structure of $[(H_2L1)^{2+}\cdot 2(H_2btrc)^{1-}]$ ***(1)***

Cocrystal **1** crystallizes as colorless cuboid-shaped crystals. The structural determination shows that it forms a 1:2 (H_2L1^{2+}:H_2btrc^{1-}) cocrystal in the triclinic P space group with $Z = 2$, the asymmetric unit consisting of one entire $(H_2L1)^{2+}$ cation and two $(H_2btrc)^{1-}$ anions (Fig. 1a). The C–O bond lengths in the 1,2,4-

Table 2 Geometrical parameters for hydrogen bonds and π–π interactions in cocrystals **1–3**

	D–H···A	D–H (Å)	H···A (Å)	D···A (Å)	< D–H···A (°)	Symmetry code
Cocrystal **1**	N2–H1A···O1	0.89 (3)	1.91 (3)	2.786 (2)	169 (2)	$2 - x, 1 - y, 1 - z$
	N4–H2A···O6	0.85 (3)	1.89 (3)	2.718 (2)	165 (3)	$1 - x, 2 - y, -z$
	O5–H5···O4	0.83 (2)	1.75 (2)	2.576 (2)	175 (3)	$-1 + x, y, z$
	C3–H3···O11	0.93	2.54	3.454 (3)	166	$-1 + x, 1 + y, z$
	C11–H11B···O8	0.97	2.27	3.214 (3)	163	
	C17–H17···O7	0.93	2.46	3.083 (3)	124	$1 + x, y, z$
	C15–H15···O8	0.93	2.53	3.313 (3)	142	$2 - x, 1 - y, -z$
	C19–H19A···O8	0.96	2.58	3.391 (3)	142	$1 - x, 1 - y, -z$
	C19–H19B···O3	0.96	2.43	3.347 (3)	159	$-1 + x, y, z$
Cocrystal **2**	N2–H2···O1	0.86 (3)	2.08 (3)	2.930 (2)	171 (3)	$1 - x, 1/2 + y, 1/2 - z$
	O1 W–H1 WA···O4	0.86	1.76	2.614 (2)	176	$1 - x, 1/2 + y, 1/2 - z$
	O1W–H1WB···O3	0.85 (2)	2.03 (2)	2.870 (2)	170 (3)	$x, y, 1 + z$
	O3–H3···O2	0.82	1.67	2.486 (2)	171	$x, 1/2 - y, -1/2 + z$
	C2–H2B···O4	0.96	2.51	3.425 (3)	158	$-x, 1 - y, -z$
	C5–H5···O4	0.93	2.46	3.253 (3)	144	$x, 1 + y, z$
Cocrystal **3**	N1–H1···O2	0.86	1.79	2.627 (2)	166	$x, y, 1 + z$
	C6–H6···O4	0.93	2.42	3.334 (3)	166	$1 - x, -i, 1 - z$
	C8–H8A···O3	0.97	2.52	3.465 (3)	165	$-1 + x, y, z$
	C10–H10···O2	0.93	2.58	3.455 (3)	156	$1 - x, -yi, 1 - z$
	C17–H17B···O3	0.96	2.36	3.306 (3)	168	$-1 + x, y, z$
Cocrystal **1**	Cg(2)[a]–Cg(4)[b]			3.609 (1)		$2 - x, 1 - y, -z$
	Cg(4)–Cg(7)[c]			3.606 (1)		x, y, z
	Cg(3)–Cg(3)[d]			3.663 (1)		$1 - x, 1 - y, 1 - z$

Table 2 continued

	D–H···A	D–H (Å)	H···A (Å)	D···A (Å)	< D–H···A (°)	Symmetry code
Cocrystal **3**	Cg(1)[e]–Cg(2)[f]			3.455 (1)		$-x, -y, 2 - z$

[a] 5-Membered ring N3–C12–N4–C13–C18

[b] 6-Membered ring C13–C14–C15–C16–C17–C18

[c] 6-Membered ring C20–C21–C22–C23–C24–C25

[d] 6-Membered ring C1–C2–C3–C4–C5–C6

[e] 5-Membered ring N1–C1–N2–C7–C2

[f] 6-Membered ring C2–C3–C4–C5–C6–C7

benzenetricarboxylic acid groups (O1–C26 = 1.235(2) Å, O2–C26 = 1.288(2) Å; O3–C27 = 1.277(2) Å, O4–C27 = 1.243(2) Å; O5–C28 = 1.306(2) Å, O6–C28 = 1.217(2) Å) indicate that the acid moiety at C26 and C28 is present as –COOH, while at C27 is present as $–COO^-$. Moreover, the $(H_2L1)^{2+}$ cation exhibits an *anti*-conformation mode with the dihedral angle of 77.927(4)° between two benzimidazole rings in an entire ligand. In cocrystal **1**, the desired N–H···O (distance of 2.786(2) Å for N2–H1A···O1, 2.718(2) Å for N4–H2A···O6) and O–H···O (2.576(2) Å for O5–H5···O4) hydrogen bond interactions are generated between H_2L1^{2+} and H_2btrc^{1-} to form a 2D sheet with an $R_6^6(48)$ motif along the crystallographic *b* axes (Fig. 1b). It is noteworthy that the 2D network are interlinked by π–π interactions to constitute a 3D supramolecular framework with face-to-face distances ranging from 3.606(1) to 3.663(1) Å (Fig. 1c).

*Crystal structure of $[(H_2L2)^{2+}\cdot(H_2btec)^{2-}\cdot 2H_2O]$ (**2**)*

Cocrystal **2** is colorless cuboid-shaped crystal. The structural determination shows it forms a 1:1:2 (H_2L2^{2+}:H_2btc^{2-}:H_2O) cocrystal in the monoclinic $P2_1/c$ space group with $Z = 2$. The asymmetric unit of **2** comprises one half of a H_2L2^{2+} cation, one half of a H_2btc^{2-} anion, and one water molecule (Fig. 2a). The C–O bond distances 1.248(2) Å (O1–C14) and 1.265(2) Å (O2–C14) are for the COO^- group. The C–O bonds (O3–C15 = 1.301(3) Å, O4–C15 = 1.218(2) Å) in the COOH show characteristic C–O, and C = O bond distances, which are confirming the reliability of adding H atoms experimentally by different electron density onto O atoms. As shown in Fig. 2b, the water molecules and H_2btc^{2-} are involved in the formation of a 2D supramolecular layer heterosynthon through O–H···O (distance of 2.614(2) Å, 2.870(2) Å, and 2.486(2) Å) hydrogen bond interactions. For the linking of these non-bonding interactions there extended into the close joint $R_4^4(24)$ and $R_2^2(13)$ motifs. In addition, the 2D sheets were further stacked by the N–H···O hydrogen bond interactions (N2–H2···O1 = 2.930(2) Å, and N2–H2···O1 = 171(3)°) between the protonated 1,4-bis(2-methylbenzimidazole)butane and partly deprotonated 1,2,4,5-benzenetetracarboxylic acids to form a 3D supramolecular structure (Fig. 2c).

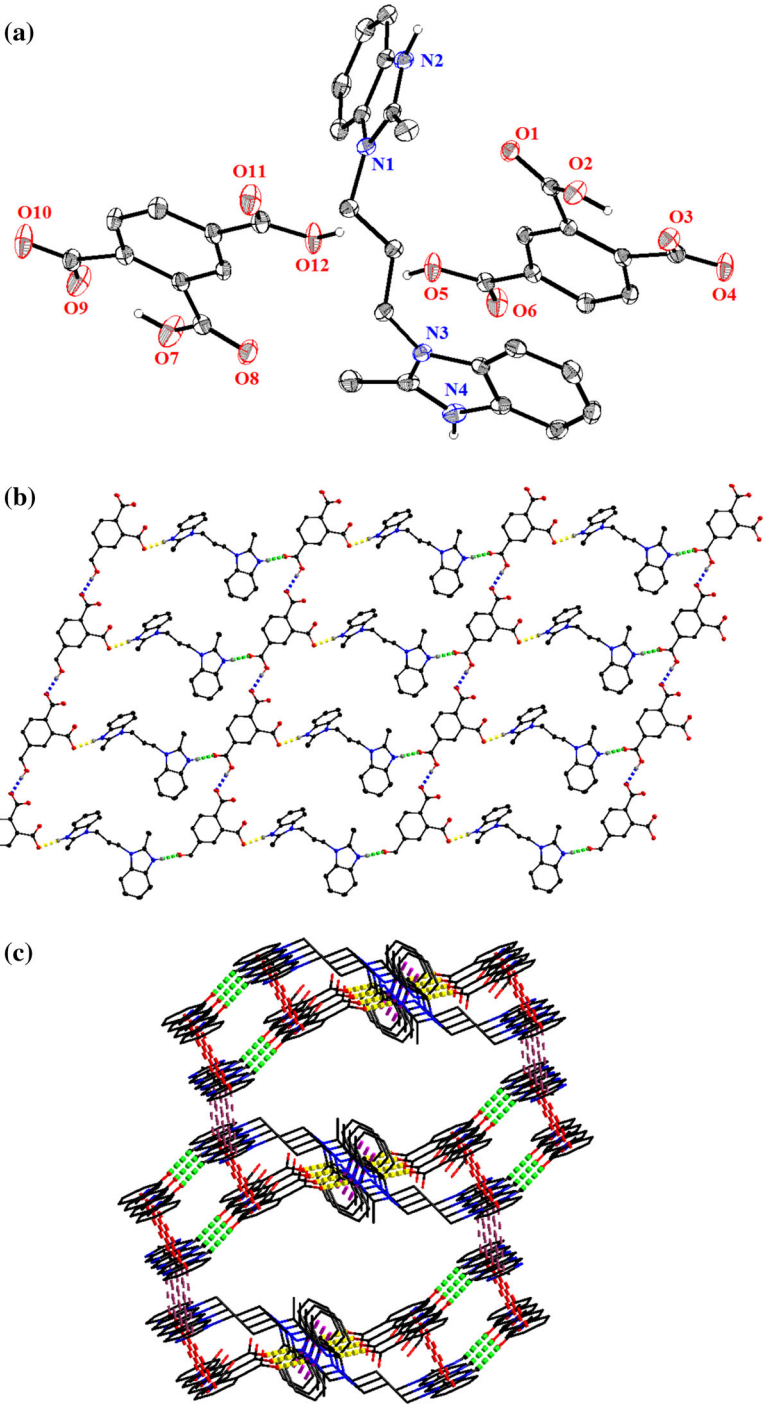
(a)
N2
N1
O1
O2
O11
O10
O12
O3
O5
O6
O4
O9
N3
O7
O8
N4
(b)
(c)

◀**Fig. 1** **a** The ORTEP figures of cocrystal **1** with 30% thermal ellipsoids. **b** The 2D sheet structure generated through hydrogen bond interactions in cocrystal **1**. **c** The 3D supramolecular framework generated through π–π interactions in cocrystal **1**

Crystal structure of $[(H_2L3)^{2+}\cdot(H_2btec)^{2-}]$ (**3**)

Cocrystal **3** crystallizes as colorless cuboid-shaped crystals, representing the triclinic *P* space group with $Z = 1$. As shown in Fig. 3a, the asymmetric unit of **3** consists of one half of a H_2L3^{2+} cation and one half of a H_2btc^{2-} anion. The 1,2,4,5-benzenetetracarboxylic acid molecule is deprotonated, which is confirmed by the pairs of bond distances of O1–C16 (1.243(3) Å), and O2–C16 (1.268(3) Å) for the carboxylate. The C–O bond distances 1.219(3) Å (O4–C15) and 1.298(3) Å (O3–C15) are for the COOH group. Meanwhile, each H_2L3^{2+} adopts *anti*-conformation with the two benzimidazole rings being in a parallel fashion. Incontrovertibly, it forms N–H···O hydrogen bond interactions between the carboxylate oxygen atoms and the protonated H_2L3^{2+} cations (N1–H1···O2 = 2.627(2) Å), which can further assemble into a 1D zigzag chain (Fig. S1). Moreover, the 1D chains were further stacked via the π–π interactions (Cg1–Cg2) between the benzimidazole and benzene rings of H_2L3^{2+} to form a 3D network structure. The centroid-to-centroid distance between imidazole and benzene ring is 3.455(1) and the corresponding dihedral angle is 0.33° (Fig. 3b).

IR spectra

The IR spectra for cocrystals **1**–**3** are shown in Fig. S2. For **2**, the peaks around 3400 cm^{-1} can be associated with the O–H stretching vibration modes of water molecules. The bands in the range of 1350–1550 cm^{-1} in **1**–**3** are mainly assigned to the asymmetric and symmetric stretching vibrations of the carboxylate groups. The strong peaks around 1700 cm^{-1} are observed, indicating that all carboxylate groups of **1**–**3** are partly deprotonated. The characteristic peaks at 1580 cm^{-1} for **1**, 1470 cm^{-1} for **2** and 1460 cm^{-1} for **3** are due to the $\nu_{(C=N)}$ stretching vibration of the benzimidazole rings. Some weak peaks at 3100 cm^{-1} for **1**, 3111 cm^{-1} for **2** and 3095 cm^{-1} for **3** are attributed to the $\nu_{(C-H)}$ stretching vibration of the benzimidazole rings [33].

Hirshfeld surface analysis

The d_{norm} Hirshfeld surfaces plotted on the studied cocrystals **1**–**3** are presented in Fig. 4. Each aromatic carboxylic acid and N-containing building blocks in the asymmetric unit of a given cocrystal structure has a unique Hirshfeld surface, which clearly displays the influences of different building blocks on the intermolecular interactions. In the Hirshfeld surfaces, the large and deep red spots are due to the close-contact interactions, and they are mainly responsible for the significant hydrogen bonding contacts, such as N–H···O and O–H···O interactions. The small circular spots (light red) visible on the surfaces indicative of C–H···O interactions.

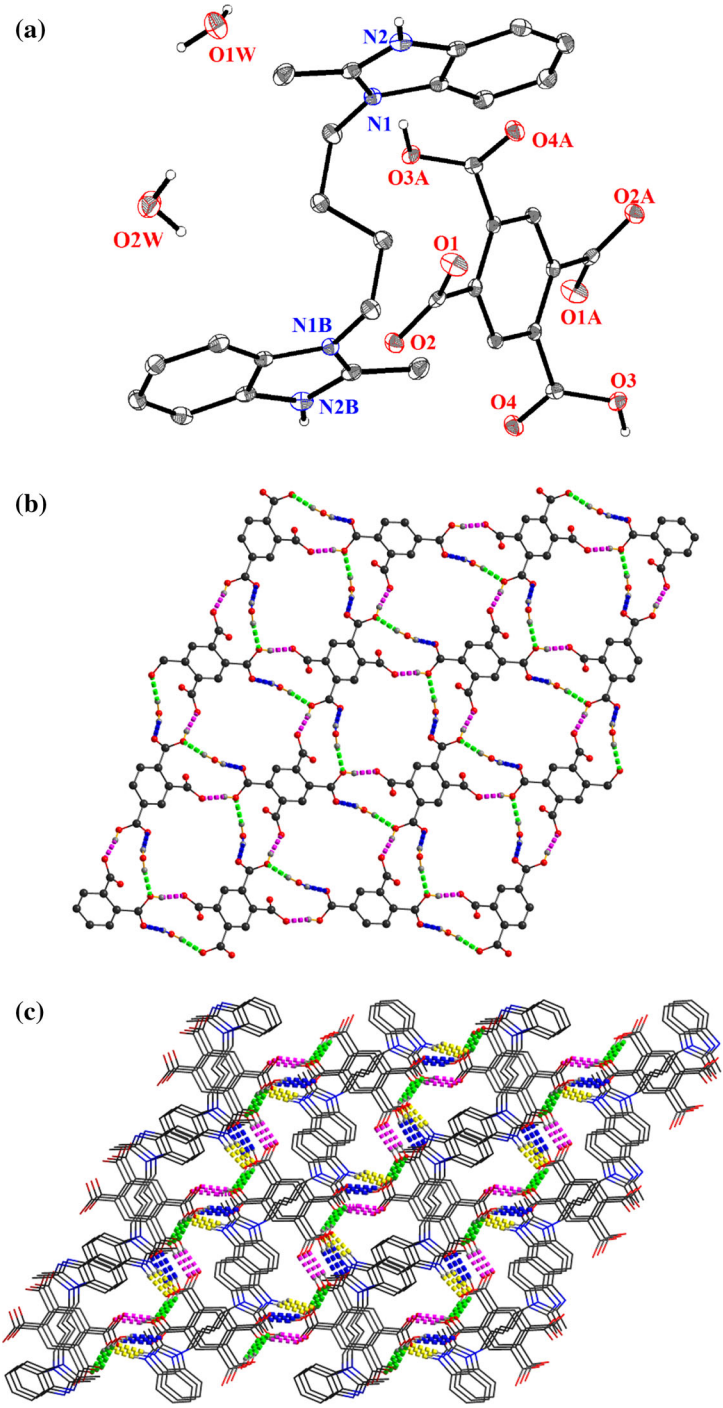
(a)
O1W
N2
N1
O4A
O3A
O2A
O2W
O1
O1A
N1B
O2
O3
O4
N2B
(b)
(c)

◀**Fig. 2** **a** The ORTEP figures of cocrystal **2** with 30% thermal ellipsoids. **b** The 2D sheet structure generated through O–H···O interactions in cocrystal **2**. **c** The 3D supramolecular framework generated through N–H···O interactions in cocrystal **2**

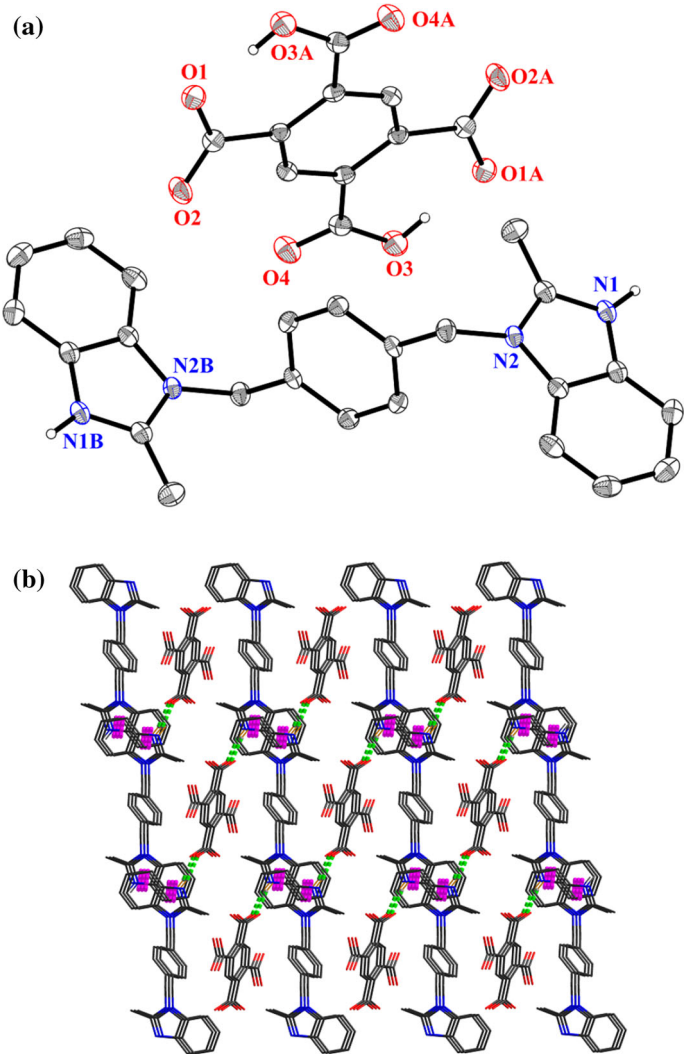

Fig. 3 **a** The ORTEP figures of cocrystal **3** with 30% thermal ellipsoids. **b** The 3D supramolecular framework generated through π–π interactions in cocrystal **3**

Other visible spots in the surfaces are because of H···H contacts. Figures 5a–c and 6a–c depict 2D fingerprint plots and percentage contributions of various intermolecular contacts for cocrystals **1–3**, respectively. The fingerprint plots can be decomposed to highlight particular atoms pair close contacts. This

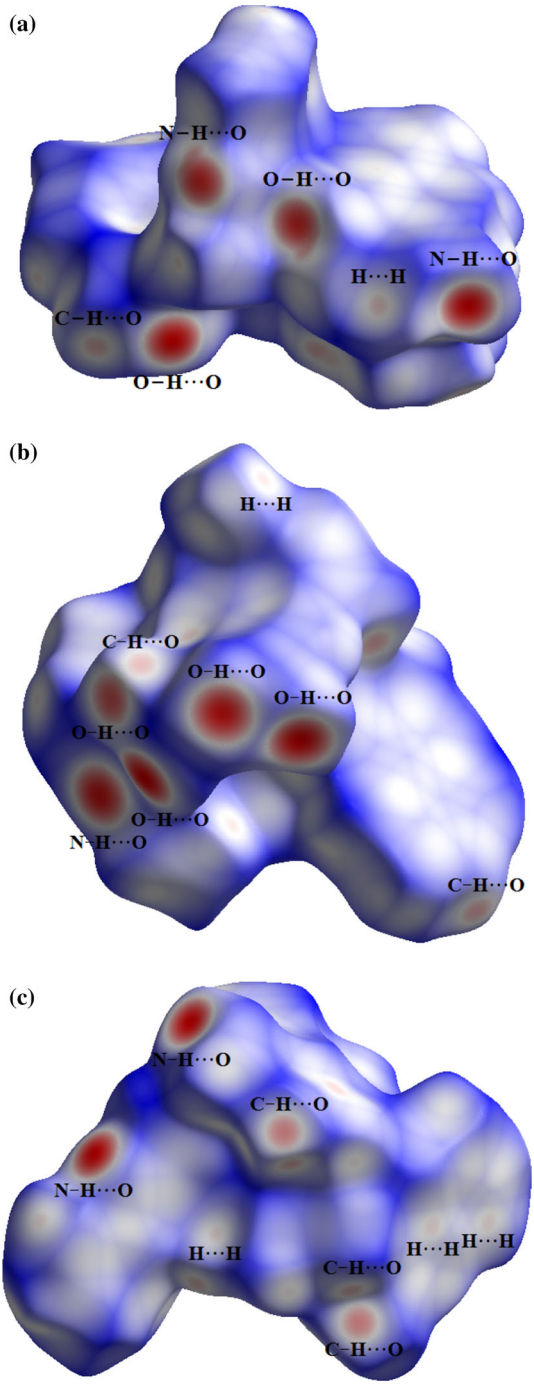

Fig. 4 **a** The Hirshfeld surface mapped with d_{norm} for cocrystal **1**. **b** The Hirshfeld surface mapped with d_{norm} for cocrystal **2**. **c** The Hirshfeld surface mapped with d_{norm} for cocrystal **3**

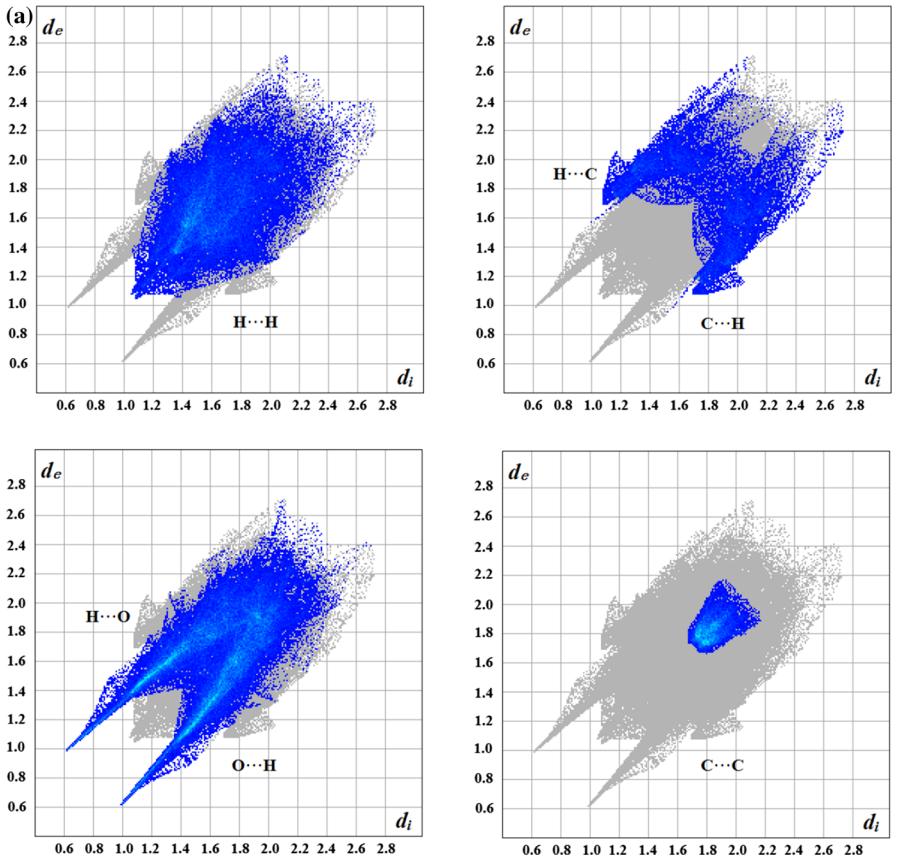

Fig. 5 **a** The 2D fingerprint plots for cocrystal **1**. **b** The 2D fingerprint plots for cocrystal **2**. **c** The 2D fingerprint plots for cocrystal **3**

decomposition enables separation of contributions from different interaction types, which overlap in the full fingerprint.

As shown in Fig. 6a–c, for all structures, the most significant proportions of contacts are observed for H···H interactions (comprising 29.2% of **1**, 37.5% of **2**, and 36.5% of **3**), which are reflected in the middle of scattered points of fingerprint plots. The proportion of C···H and H···C interactions, reflected as points at the regions of bottom right ($d_e < d_i$, C···H) and top left ($d_e > d_i$, H···C), have 14.0% contribution to the total Hirshfeld surfaces for **1**, 12.5% for **2,** and 13.4% for **3**, while the proportion of O···H and H···O contacts comprise 42.9, 41.5, and 35.8% of the Hirshfeld surfaces for each molecule in **1**, **2,** and **3**, respectively. The significant π···π interactions are also observed, with the C···C close interactions comprised of 6.4% in **1**, 3.8% in **2,** and 6.2% in **3**.

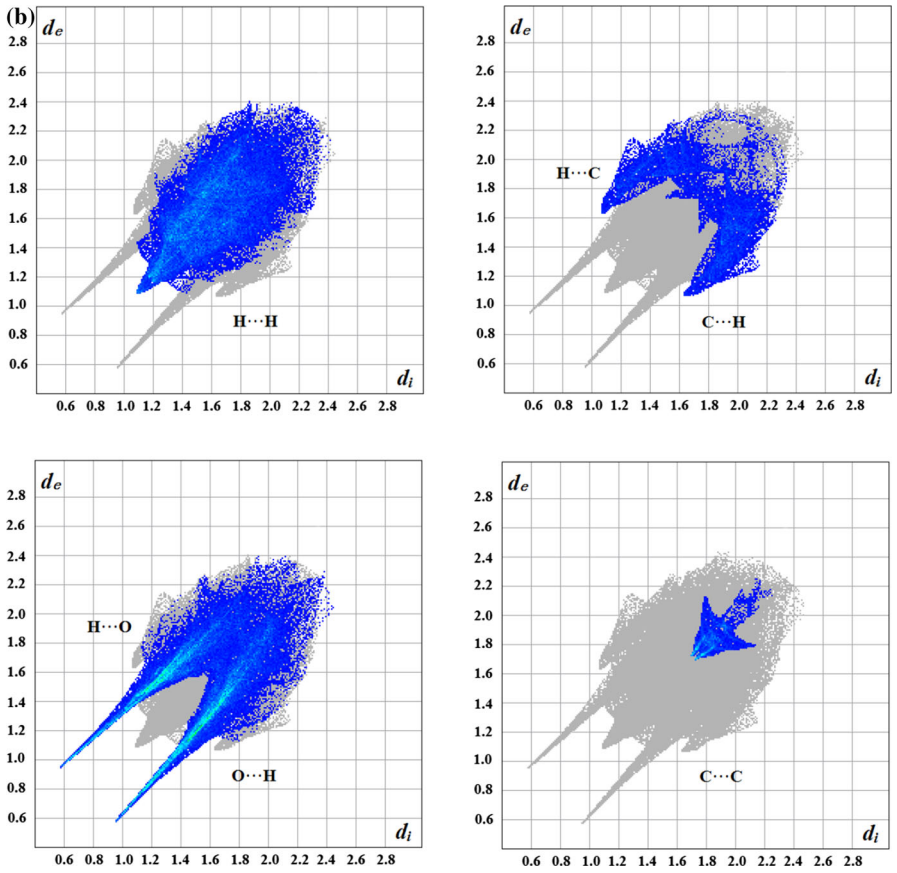

Fig. 5 continued

Thermal properties

The thermal properties of cocrystals **1**–**3** were examined by thermogravimetric (TG) analysis under N_2 atmosphere with a heating rate of 10 °C·min^{-1} in temperature range from room temperature to 800 °C. The TG curves show that both **1** and **3** own one weight loss step, while **2** possesses two distinct steps of weight loss (Fig. 7). For **1**, the weight loss of 99.30% occurs in the temperature range of 273 and 572 °C, corresponding to the decomposition of the $(H_2L1)^{2+}$ cations and $(H_2btrc)^{1-}$ anions. For **2**, the decomposition of lattice water molecules (found. 5.81%, calcd. 5.92%) in the first step is observed between 90 and 156 °C. The second weight loss from 264 to 600 °C can be attributed to the decomposition of molecular components $(H_2L2)^{2+}$ and $(H_2btec)^{2-}$. Cocrystal **3** starts to decompose with the weight loss of 99.60% below 249 °C, which may result from the release of $(H_2L3)^{2+}$ and $(H_2btec)^{2-}$.

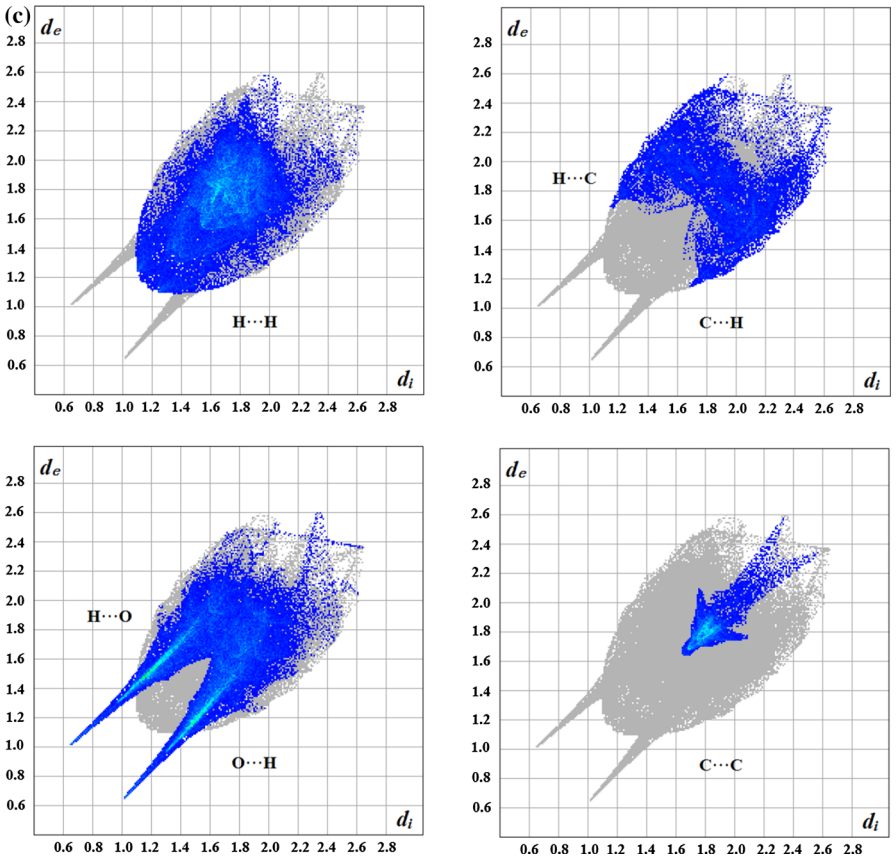

Fig. 5 continued

Photoluminescent properties

The solid-state photoluminescence spectra of cocrystals **1**–**3** and the corresponding molecular components were recorded at room temperature. As shown in Fig. 8, the free L1, L2, L3, H_3btrc, and H_4btec show strong emission maxima at 349, 369, 390, 424, and 412 nm upon excitation at 310, 300, 250, 290, and 265 nm, respectively, which is attributed to $n \rightarrow \pi^*$ or $\pi \rightarrow \pi^*$ transition [34]. Cocrystals **1**–**3** display similar fluorescent emissions bands at 396 nm for **1** ($\lambda_{ex} = 260$ nm), 397 nm for **2** ($\lambda_{ex} = 260$ nm), and 396 nm for **3** ($\lambda_{ex} = 260$ nm), respectively. In comparison with free L1, L2, and L3, the emission maxima of cocrystals **1**, **2**, and **3** are red-shifted (47 nm for **1**, 28 nm for **2**, 6 nm for **3**), which may be caused by hydrogen bonding between the molecular components [35–38]. Additionally, the emission of **1**–**3** all show a slight blue shift (28 nm for **1**, 15 nm for **2**, 16 nm for **3**) relative to the H_3btrc and H_4btec, respectively, which is probably due to the $\pi \rightarrow \pi^*$ intraligand transitions because of their close resemblance to the emission band of the corresponding aromatic carboxylic acids.

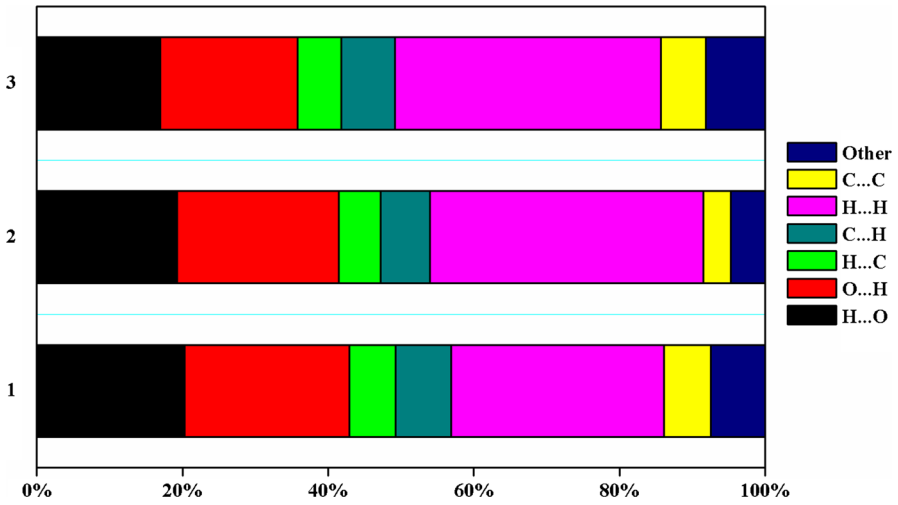

Fig. 6 The relative percentage contributions to the Hirshfeld surface area for various intermolecular contacts in cocrystals **1–3**

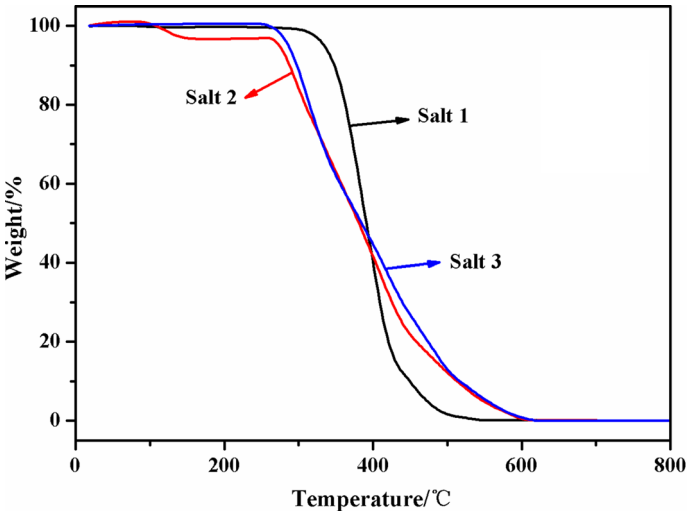

Fig. 7 TG curves of cocrystals **1–3** in N_2 atmosphere

Conclusion

In summary, three new cocrystals based on bis(benzimidazole) derivatives and aromatic carboxylic acids have been successfully synthesized and characterized. The results of the single-crystal structure analysis and Hirshfeld surfaces reveal that molecular components in **1** link each other through N–H···O and O–H···O interactions to generate a 2D sheet which is further extended into a 3D supremolecular framework via π–π interactions. For **2**, the water molecules and

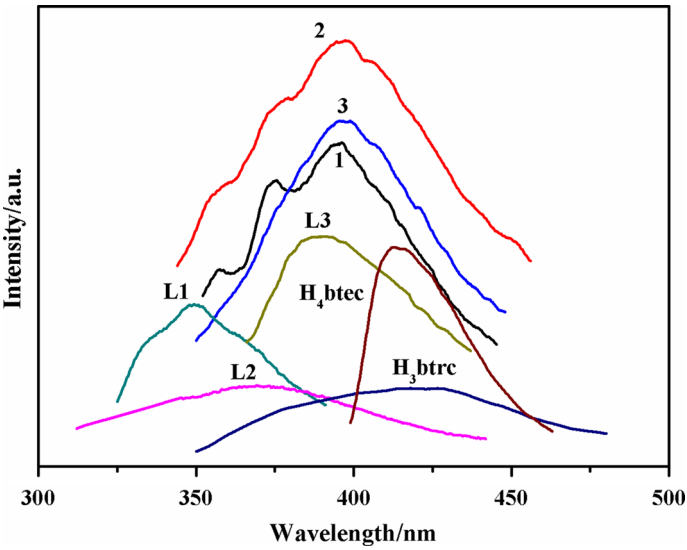

Fig. 8 The fluorescence spectra of cocrystals **1–3** and molecular components

H_2btc^{2-} cations are involved in the formation of a 2D layer heterosynthon by O–H···O contacts, then form a 3D supramolecular structure through N–H···O hydrogen bond interactions. Cocrystal **3** displays an infinite zigzag chain structure, which is further assembled into a 3D supramolecular structure via π–π interactions, respectively. In addition, three cocrystals possess interesting photoluminescence properties in the solid state.

Supplementary data

CCDC 1482021, 1482022 and 1482023 contain the supplementary crystallographic data for cocrystals **1–3**. These data can be obtained free of charge via http://www.ccdc.cam.ac.uk/conts/retrieving.html, or from the Cambridge Crystallographic Data Centre, 12 Union Road, Cambridge CB21EZ, UK; fax: (+44) 1223-336-033; or e-mail: deposit@ccdc.cam.ac.uk.

Acknowledgements The project was supported by the National Natural Science Foundation of China (51474086), Natural Science Foundation – Steel and Iron Foundation of Hebei Province (B2015209299).

References

1. G.G. Hou, J.P. Ma, L. Wang, P. Wang, Y.B. Dong, R.Q. Huang, CrystEngComm **12**, 4287 (2010)
2. N. Takata, K. Shiraki, R. Takano, Y. Hayashi, K. Terada, Cryst. Growth Des. **8**, 3032 (2008)
3. J. Rebek, Angew. Chem. Int. Ed. **44**, 2068 (2005)
4. M. Lou, S.H. Mao, Y.H. Luo, P. Zhao, B.W. Sun, Res. Chem. Intermed. **41**, 2939 (2015)
5. C.B. Aakeroy, K.R. Seddon, Chem. Soc. Rev. **22**, 397 (1993)

6. D.S. Lawrence, T. Jianf, M. Levett, Chem. Rev. **95**, 2229 (1995)
7. T. Basu, H.A. Sparkes, R. Mondal, Cryst. Growth Des. **9**, 5164 (2009)
8. M.S. Fonari, E.V. Ganin, S.S. Basok, K.A. Lyssenko, M.J. Zaworotko, V.C. Kravtsov, Cryst. Growth Des. **10**, 5210 (2010)
9. L.R. MacGillivray, J.L. Atwood, J. Solid State Chem. **152**, 199 (2000)
10. B. Moulton, M.J. Zaworotko, Chem. Rev. **101**, 1629 (2001)
11. Q.L. Liu, L.J. Yang, Y.H. Luo, Y.H. Jiang, B.W. Sun, Res. Chem. Intermed. **42**, 6947 (2016)
12. J.H. Ter Horst, M.A. Deij, P.W. Cains, Cryst. Growth Des. **9**, 1531 (2009)
13. A.L. Gavrilova, B. Bosnich, Chem. Rev. **104**, 349 (2004)
14. P. Kopel, D. Wawrzak, V. Langer, K. Cihalova, D. Chudobova, R. Vesely, V. Adam, R. Kizek, Molecules **20**, 10360 (2015)
15. L.H. Zhai, L.H. Guo, Y. Ling, H.S. Wu, J.W. Wang, B.W. Sun, Y.H. Luo, Res. Chem. Intermed. **43**, 817 (2017)
16. C.B. Aakeröy, D.J. Salmon, B. Leonard, J.F. Urbina, Cryst. Growth Des. **5**, 865 (2005)
17. C.B. Aakeröy, D.J. Salmon, M.M. Smith, J. Desper, Cryst. Growth Des. **6**, 1033 (2006)
18. S. Jin, H. Zhang, H. Liu, X. Wen, M. Li, D. Wang, J. Mol. Struct. **1096**, 157 (2015)
19. X.X. Wang, Y.J. Ma, H.H. Li, G.H. Cui, Transit. Met. Chem. **40**, 99 (2014)
20. X. Zhang, G.Y. Dong, Y.G. Liu, G.H. Cui, J. Inorg. Organomet. Polym Mater. **26**, 62 (2015)
21. K. Sumida, M.L. Foo, S. Horike, J.R. Long, Eur. J. Inorg. Chem. **2010**, 3739 (2010)
22. H. Jiang, Y.Y. Liu, J.F. Ma, W.L. Zhang, J. Yang, Polyhedron **27**, 2595 (2008)
23. L. Liu, Y.H. Liu, G. Han, D.Q. Wu, H.W. Hou, Y.T. Fan, Inorg. Chim. Acta **403**, 25 (2013)
24. M. Du, Z.H. Zhang, X.J. Zhao, Cryst. Growth Des. **5**, 1199 (2005)
25. S. Aitipamula, R. Banerjee, A.K. Bansal, K. Biradha, M.L. Cheney, A.R. Choudhury, G.R. Desiraju, A.G. Dikundwar, R. Dubey, N. Duggirala, P.P. Ghogale, S. Ghosh, P.K. Goswami, N.R. Goud, R.R.K.R. Jetti, P. Karpinski, P. Kaushik, D. Kumar, V. Kumar, B. Moulton, A. Mukherjee, G. Mukherjee, A.S. Myerson, V. Puri, A. Ramanan, T. Rajamannar, C.M. Reddy, N. RodriguezHornedo, R.D. Rogers, T.N.G. Row, P. Sanphui, N. Shan, G. Shete, A. Singh, C.C. Sun, J.A. Swift, R. Thaimattam, T.S. Thakur, R. Kumar Thaper, S.P. Thomas, S. Tothadi, V.R. Vangala, N. Variankaval, P. Vishweshwar, D.R. Weyna, M.J. Zaworotko, Cryst. Growth Des. **12**, 2147 (2012)
26. M.A. Spackman, J.J. McKinnon, CrystEngComm **4**, 378 (2002)
27. M.A. Spackman, D. Jayatilaka, CrystEngComm **11**, 19 (2009)
28. W. Wang, Y. Ling, L.J. Yang, Q.L. Liu, Y.H. Luo, B.W. Sun, Res. Chem. Intermed. **42**, 3157 (2016)
29. A. Parkin, G. Barr, W. Dong, C.J. Gilmore, D. Jayatilaka, J.J. Mckinnon, M.A. Spackman, C.C. Wilson, CrystEngComm **9**, 648 (2007)
30. G.M. Sheldrick, Acta Crystallog. Sect. A **64**, 112 (2008)
31. F.L. Hirshfeld, Theor. Chim. Acta **44**, 129 (1977)
32. S.K. Wolff, D.J. Grimwood, J.J. McKinnon, M.J. Turner, D. Jayatilaka, M.A. Spackman, CrystalExplorer 3.1; University of Western Australia: Crawley, Australia (2013)
33. X.X. Wang, B. Yu, K. Van Hecke, G.H. Cui, RSC Adv. **4**, 61281 (2014)
34. H.Y. Liu, H. Wu, J.F. Ma, Y.Y. Liu, B. Liu, J. Yang, Cryst. Growth Des. **10**, 4795 (2010)
35. Y.H. Ma, M. Lou, Q.Y. Sun, S.W. Ge, B.W. Sun, J. Mol. Struct. **1083**, 111 (2015)
36. J.W. Cui, S.X. Hou, K. Van Hecke, G.H. Cui, Dalton Trans. **46**, 2892 (2017)
37. X. Zhang, Y.Q. Zhao, F.S. Wang, G.Y. Dong, J. Struct. Chem. **35**, 765 (2016)
38. J.M. Hu, V.A. Blatov, B.Y. Yu, K. Van Hecke, G.H. Cui, Dalton Trans. **45**, 2426 (2016)